nature biotechnology

Chaperones as thermodynamic sensors of drug-target interactions reveal kinase inhibitor specificities in living cells

Mikko Taipale[1], Irina Krykbaeva[1], Luke Whitesell[1], Sandro Santagata[1,2], Jianming Zhang[3], Qingsong Liu[3], Nathanael S Gray[3] & Susan Lindquist[1,4,5]

The interaction between the HSP90 chaperone and its client kinases is sensitive to the conformational status of the kinase, and stabilization of the kinase fold by small molecules strongly decreases chaperone interaction. Here we exploit this observation and assay small-molecule binding to kinases in living cells, using chaperones as 'thermodynamic sensors'. The method allows determination of target specificities of both ATP-competitive and allosteric inhibitors in the kinases' native cellular context in high throughput. We profile target specificities of 30 diverse kinase inhibitors against >300 kinases. Demonstrating the value of the assay, we identify ETV6-NTRK3 as a target of the FDA-approved drug crizotinib (Xalkori). Crizotinib inhibits proliferation of ETV6-NTRK3-dependent tumor cells with nanomolar potency and induces the regression of established tumor xenografts in mice. Finally, we show that our approach is applicable to other chaperone and target classes by assaying HSP70/steroid hormone receptor and CDC37/kinase interactions, suggesting that chaperone interactions will have broad application in detecting drug-target interactions *in vivo*.

Determining the specificity of small molecules is important for research scientists, medicinal chemists, clinicians and their patients alike. In the laboratory, small-molecule drugs are commonly used as chemical probes, and the meaningful interpretation of the results of such experiments requires detailed knowledge of a drug's targets. In the pharmaceutical industry, target profiling can be used to identify candidate targets for compounds discovered in cell-based screens and to guide medicinal chemistry efforts to obtain a favorable target spectrum during lead compound optimization. In the clinic, experimental drugs often show unexpected efficacy or toxicity that can sometimes be explained through more thorough target profiling. Moreover, identification of additional targets of an approved drug with a previously established safety profile can facilitate its rapid repurposing to new diseases.

The protein kinase family illustrates the challenges inherent to target profiling. Almost all protein kinases share the same conserved fold, and, consequently, developing inhibitors that are both highly potent and highly selective has proven difficult[1,2]. Given the pharmaceutical interest in drugging protein kinases, several high-throughput methods have been developed for profiling inhibitor specificities *in vitro*[3–8]. However, the correlation between *in vitro* results and *in vivo* efficacy has often been disappointing[9,10]. Chemical proteomics-based approaches have shown considerable promise for inhibitor profiling[11,12]. However, they are not well suited to profiling allosteric inhibitors, which are not competitive with the ATP site–directed labeling agents employed by these methods.

Currently, no assays combine the benefits of *in vitro* assays (high throughput) with those of *in vivo* approaches (relevant cellular context). We recently developed a quantitative protein-protein interaction assay to survey the association of the HSP90 chaperone and its CDC37 co-chaperone with the majority of human kinases *in vivo*[1]. We established that one of the main determinants of HSP90's association with a particular kinase is the thermal stability of the kinase domain. Here, we exploit this finding and use HSP90 and CDC37 as thermodynamic sensors for profiling small molecule–kinase interactions in living cells. We further demonstrate that this assay is not limited to kinases as targets and HSP90 or CDC37 as sensors, suggesting a more general approach for probing small molecule–target interactions.

RESULTS

Characterizing ATP-competitive kinase inhibitors *in vivo*

To study HSP90–client protein interactions in a systematic manner, we developed an assay derived from the luminescence-based mammalian interactome (LUMIER) assay[13]. Our implementation, LUMIER with bait control (BACON), both increases the assay throughput and enables quantification of interactions[1]. Briefly, the assay employs 293T cells stably expressing the chaperone protein HSP90 fused to *Renilla* luciferase. Plasmids encoding potential client proteins (e.g., kinases, transcription factors and ubiquitin ligases) with a 3xFLAG epitope tag are then used to transiently transfect the cell line expressing luciferase-tagged HSP90. The interaction of client proteins with

[1]Whitehead Institute for Biomedical Research, Cambridge, Massachusetts, USA. [2]Department of Pathology, Brigham and Women's Hospital and Harvard Medical School, Boston, Massachusetts, USA. [3]Department of Biological Chemistry & Molecular Pharmacology, Harvard Medical School and Department of Cancer Biology, Dana-Farber Cancer Institute, Boston, Massachusetts, USA. [4]Department of Biology, Massachusetts Institute of Technology, Cambridge, Massachusetts, USA. [5]Howard Hughes Medical Institute, Cambridge, Massachusetts, USA. Correspondence should be addressed to S.L. (lindquist_admin@wi.mit.edu).

Received 26 November 2012; accepted 22 May 2013; published online 30 June 2013; doi:10.1038/nbt.2620

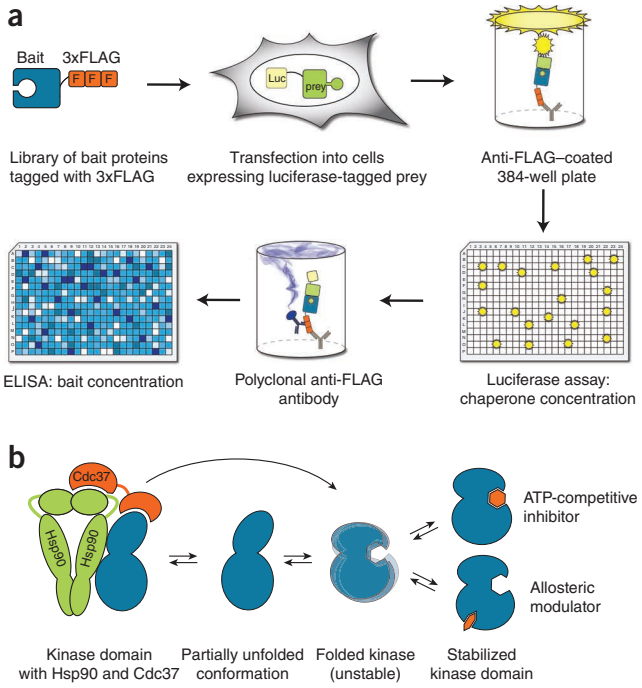

Figure 1 Principle of the chaperone assay. (**a**) LUMIER with BACON assay. Chaperone-*Renilla* luciferase fusion protein is stably expressed in 293T cells. 3xFLAG-tagged bait proteins are transfected into the cell line in 96-well format, and the cell lysates expressing each bait protein are applied to anti-FLAG coated 384-well plates. The amount of luminescence in the well after washing off nonspecifically binding proteins indicates the amount of co-purified chaperone. After the luminescence measurement, the amount of bait protein is measured with ELISA, using a different, polyclonal anti-FLAG antibody coupled to horseradish peroxidase. The interaction score is calculated as $\log_2$[chaperone/bait]. (**b**) Protein kinases are in equilibrium between the fully folded conformation and a partially unfolded conformation that is recognized by Hsp90 and its kinase-specific co-chaperone Cdc37. Hsp90 machinery assists the kinase in adopting its fully folded conformation. Binding of a small molecule to the kinase fold shifts the equilibrium toward the fully folded conformation, which can be detected as decreased chaperone interaction.

the luciferase-tagged HSP90 is detected in cell lysates by immunoprecipitation with anti-FLAG antibodies in 384-well plates and quantification of the luminescence signal from the luciferase-HSP90 fusion co-purified with the FLAG-tagged client proteins. Subsequently, client protein abundance is measured by enzyme-linked immunosorbent assay (ELISA), using a polyclonal anti-FLAG antibody. Finally, the quantitative interaction score is calculated as the ratio of the luminescence (chaperone abundance) to the ELISA signals (client abundance) (**Fig. 1a**).

Previously, we found that small molecules targeting ABL kinase lead to a decrease in the interaction between BCR-ABL and HSP90 (ref. 1). Small-molecule binding stabilizes the kinase in its fully folded conformation and thereby decreases the concentration of the partially unfolded conformation that HSP90 recognizes with its co-chaperone CDC37 (**Fig. 1b**). Here, we asked whether this method provides a means to assess the potencies of specific inhibitors quantitatively *in vivo*. To provide a well-studied test set, we measured the interaction of several BCR-ABL variants with HSP90 as a function of inhibitor concentration. Cells stably expressing the *Renilla*-HSP90 fusion were transfected with different BCR-ABL constructs and treated in triplicate with increasing concentrations of inhibitors for 1 h before analysis. (**Fig. 2a–d**).

The potencies of each of the compounds in disrupting the HSP90 BCR-ABL interaction closely correlated with the known potencies of the compounds *in vivo*. Imatinib (Gleevec), the first-in-class BCR-ABL inhibitor that binds in the ATP pocket, displaced HSP90 from BCR-ABL with a half-maximal effective concentration (EC_{50}) of 180 nM. Dasatinib (Sprycel), a second-generation inhibitor, was considerably more potent (EC_{50}: 6 nM)[14]. Neither inhibitor had an effect on the interaction between HSP90 and a BCR-ABL variant that carries an isoleucine-to-threonine substitution at residue 315 (T315I). The change in this 'gatekeeper' residue of the ATP-binding pocket confers resistance to both inhibitors (**Fig. 2b**,**c**)[14]. By contrast, the third-generation inhibitor ponatinib (Iclusig), specifically developed to combat the gatekeeper mutant[15], affected the interaction not only of the native BCR-ABL with HSP90 but also of the BCR-ABL variant with the gatekeeper mutation. Moreover, in keeping with previous findings on the relative potency of the compound, ponatinib displaced the mutant protein from HSP90 with fivefold lower potency (70 nM versus 22 nM) than it displaced the native BCR-ABL (**Fig. 2d**).

Kinase inhibitor treatment decreased the kinase-HSP90 interaction, without eliminating it completely. Many factors probably contribute to the residual binding in the presence of the inhibitor. First, the HSP90 chaperone cycle is complex and the client kinase may vary in its sensitivity to inhibitor at various points in its maturation[1]. Second, the degree of thermal stabilization by a small molecule depends on many factors[16] and even when a kinase is stabilized by a small molecule, it will occasionally unfold

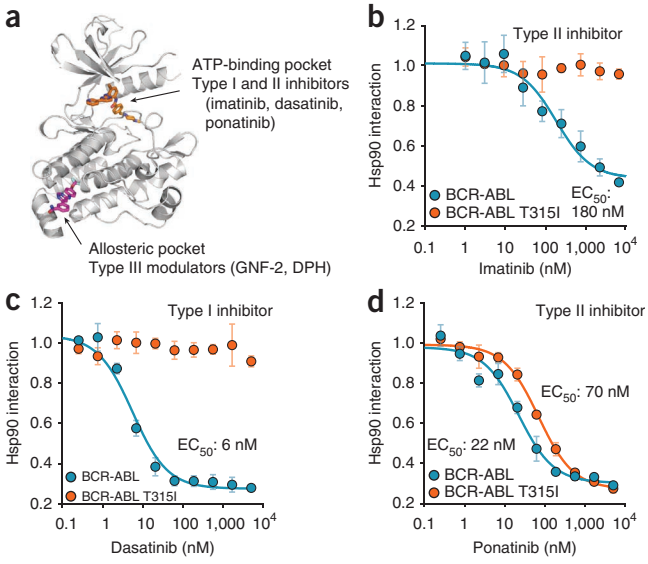

Figure 2 Characterization of ATP-competitive ABL inhibitor potencies with the chaperone interaction assay. (**a**) ABL1 and BCR-ABL can be targeted by two distinct mechanisms. Type I and II ATP-competitive inhibitors, such as imatinib (orange), bind the ATP-binding cleft, whereas allosteric modulators (type III; GNF-2, magenta) bind the myristate-binding pocket in the kinase C-terminal lobe. Figure adapted from PDB entry 3K5V. (**b**–**d**) Analysis of kinase inhibitor potencies with the chaperone interaction assay. 293T cells stably expressing *Renilla* luciferase-Hsp90 fusion protein were transfected by 3xFLAG-tagged native BCR-ABL and the gatekeeper mutant T315I. Cells were treated with increasing concentrations of inhibitors for 1 h before cell lysis and the LUMIER assay. Treatment of cells with type II inhibitors imatinib (**b**) and ponatinib (**d**) or type I inhibitor dasatinib (**c**) led to decreased BCR-ABL–HSP90 interaction. To obtain inhibitor EC_{50} values, we fitted relative Hsp90 interaction values (no inhibitor = 1) to a three-parameter dissociation curve with Graphpad Prism. Error bars, mean ± s.d.

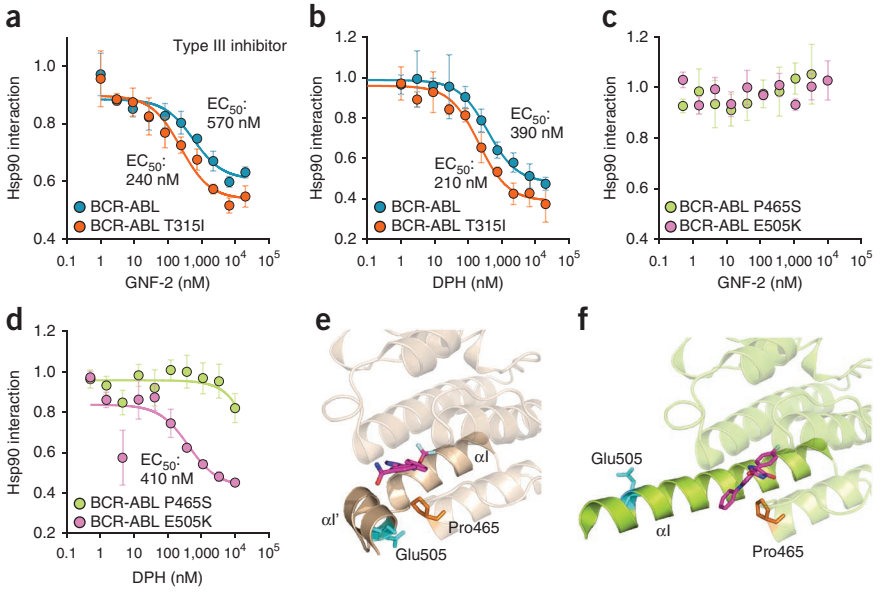

Figure 3 Characterizing allosteric ABL modulators with the chaperone interaction assay. (**a**–**d**) Analysis of kinase inhibitor potencies with the chaperone interaction assay. 3xFLAG-tagged native BCR-ABL and its mutant variants transfected 293T cells stably expressing *Renilla* luciferase-Hsp90 fusion protein. Cells were treated with increasing concentrations of inhibitors for 1 h before cell lysis and the LUMIER assay. Allosteric compounds GNF-2 (an inhibitor) and DPH (an activator) displaced HSP90 from both the native BCR-ABL and the gatekeeper mutant T315I (**a**,**b**). In contrast, mutations in the allosteric myristate-binding pocket had distinct effects on DPH and GNF-2 (**c**,**d**). P465S conferred resistance against both DPH and GNF-2, whereas E505K conferred resistance against only GNF-2. Error bars, mean ± s.d. (**e**,**f**) Structural analysis of ABL illuminates the distinct effects of myr-pocket mutations P465S and E505K on GNF-2 and DPH. In the GNF-2-bound autoinhibited conformation (**e**), ABL1 αI helix (solid, champagne-colored helix) is bent 90°, bringing Glu505 (cyan) into close proximity with the myristate-binding pocket where GNF-2 (magenta) binds. Pro465 (orange) is located in the mouth of the binding pocket. The structure is based on PDB entry 3K5V. In the DPH-bound conformation (**f**), αI (solid green helix) is extended and Glu505 (cyan) is solvent-accessible. In contrast, Pro465 (orange) is in the same conformation as in the GNF-2 bound state. DPH, magenta. The structure is based on PDB entry 3PYY.

and rebind HSP90. Finally, for some kinases the chaperone binding equilibrium might not be achieved in the 1-h treatment we used. In any case, these factors should not change the EC_{50} values derived from the assay.

In all of the above experiments, the compounds were added to the growth medium for 1 h before cell lysis and the LUMIER assay. By contrast, the compounds had no effect on BCR-ABL–HSP90 interactions if they were added after lysis (**Supplementary Fig. 1**). Under the assay conditions we employed, once the cells were lysed, the HSP90 chaperone cycle was arrested owing to low temperature, the absence of nucleotides and the presence of molybdate, which is known to stabilize HSP90-client interactions[1]. Furthermore, it is unlikely that kinase inhibitors would bind the kinase when it is bound to HSP90 *in vitro*; structural studies suggest that the kinase is partially unfolded when bound to the chaperone complex[17]. Thus, although the assay readout occurs in lysates, it reflects the folding state of the kinase *in vivo* before lysis. The assay thus effectively measures the thermodynamic stabilization of the kinase fold in living cells.

Determining potencies of allosteric small-molecule modulators

Allosteric inhibitors may be preferable to ATP-competitive inhibitors because their binding sites show a larger structural variability than the conserved ATP-binding site and therefore present much greater opportunities for achieving specificity. The difficulty of developing assays that accurately reflect *in vivo* kinase regulatory interactions has greatly hindered efforts to develop allosteric inhibitors. We therefore tested the ability of the HSP90-kinase interaction to quantitatively assess the effects of two reported allosteric modulators of the ABL kinase: GNF-2 and DPH[18,19]. Both compounds bind the myristate-binding (myr) pocket located in the C-terminal lobe of ABL (**Fig. 3a**), but they have opposing effects on ABL kinase activity—GNF-2 is an inhibitor, DPH an activator[18,19].

Both GNF-2 and DPH displaced HSP90 from BCR-ABL with potencies in close agreement with their reported cellular potencies against BCR-ABL–dependent proliferation[18–20] (**Fig. 3a**,**b**). Notably, the T315I mutation, located in the ATP-binding cleft and far from the myr-pocket, did not affect the ability of either compound to displace HSP90. By contrast, a point mutation (P465S) located in the myr-pocket virtually abolished the effect of GNF-2 and DPH on HSP90's interaction with BCR-ABL (**Fig. 3c**,**d**). Consistent with this, P465S confers strong resistance against GNF-2 *in vivo*[18].

Another mutation in the myr-pocket (E505K) responded differently to GNF-2 and DPH. The E505K:HSP90 interaction was not sensitive to GNF-2, whereas it was sensitive to DPH (**Fig. 3c**,**d**). To date, no mutations have been reported to have distinct effects on allosteric modulators of ABL. To investigate the molecular basis of these results, we compared the published crystal structures of ABL bound to GNF-2 and to DPH[18,19]. In the GNF-2–bound conformation, Glu505 is adjacent to the myr pocket, and E505K confers resistance against GNF-2 *in vivo* (**Fig. 3e**)[18]. In the DPH-bound conformation, the αI helix is extended, moving Glu505 away from the binding site[19] (**Fig. 3f**). Pro465 is located in the mouth of the binding pocket in both conformations. Thus, our chaperone assay not only yielded quantitative assessment of the allosteric drug target binding affinities, but also provided evidence for qualitatively distinct binding modes.

Expanding the scope of the chaperone assay

About 40% of human kinases do not associate with HSP90 (ref. 1), and therefore they cannot be currently assayed with our method. Might they be engineered to do so? In recognizing its clients, HSP90 does not bind particular sequence motifs but, rather, associates with intrinsically unstable kinase conformations. Yet, to be recognized as clients, the kinases must still have a recognizable kinase fold[1]. Thus, mutations that globally destabilize the client would not likely work. We therefore introduced more strategic mutations into two human kinases that are normally at the limits of detection by our assay, SRC and EGFR. For EGFR, we engineered a mutation in the αC-β4 loop (D770G), which was previously reported to increase EGFR-HSP90 interaction[21]. For SRC, we introduced a mutation in an exposed glutamic acid residue at the end of the αE helix (E381K). In both cases, the mutation increased the kinase's interaction with HSP90 and the

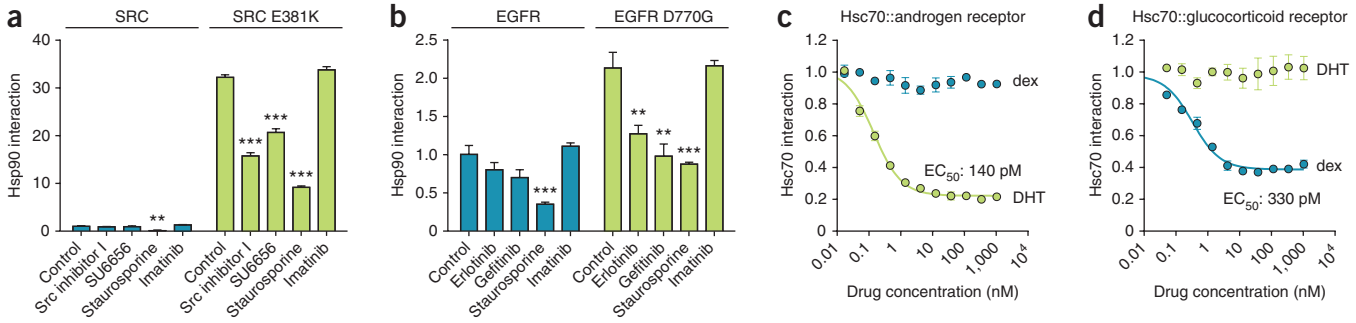

Figure 4 Expanding the scope of the chaperone interaction assay. (**a**) SRC does not appreciably associate with HSP90 in LUMIER assay, and thus, binding of the SRC-specific inhibitors SU6656 and Src inhibitor I to the kinase cannot be measured with LUMIER. Increasing SRC-HSP90 interaction by introducing a point mutation (E381K) to SRC kinase domain enables the detection of SU6656 and Src inhibitor I binding to the kinase. Inhibitors (10 μM) were added to the cells for 1 h before cell lysis and the LUMIER assay. Interaction scores correspond to relative interactions (wild-type SRC with no inhibitor = 1) ± s.d. ($n = 4$). Statistical test for significance was unpaired *t*-test with unequal variance. $^{**}P < 0.01$; $^{***}P < 0.001$. (**b**) Wild-type EGFR associates with HSP90 only weakly. Increasing its interaction with HSP90 with an aspartic acid-to-glycine mutation (D770G) facilitates the detection of binding of the EGFR-specific inhibitors erlotinib (Tarceva) and gefitinib (Iressa) to EGFR. Experiment was performed as in **a**. $^{**}P < 0.01$; $^{***}P < 0.001$. (**c**,**d**) 293T cells stably expressing *Renilla*-Hsc70 (HSPA8) were transfected with 3xFLAG tagged androgen receptor (**c**) or glucocorticoid receptor (**d**). Cells were treated with increasing concentrations of dexamethasone or dihydrotestosterone (DHT) for 1 h before cell lysis and LUMIER assay. Relative HSPA8 interaction values (no inhibitor = 1) were fitted to a three-parameter dissociation curve with Graphpad Prism. Error bars, mean ± s.d.

interactions were sensitive to EGFR and SRC kinase inhibitors, respectively (**Fig. 4a**,**b**). They remained resistant to imatinib, which does not target either kinase. Thus, with simple engineering, the assay can be readily extended to kinases that are not normally HSP90 clients.

To determine whether other chaperones could be used as *in vivo* sensors for the drug-target interactions, we first turned to CDC37. CDC37 is a kinase-specific co-chaperone for HSP90 and its interaction profile strongly correlates with that of HSP90 (ref. 1). We used a cell line stably transfected with a CDC37-*Renilla* fusion and assayed the EC_{50} of imatinib and dasatinib for BCR-ABL in a manner analogous to our *Renilla*-HSP90 sensor. Consistent with CDC37's central role in chaperoning kinases, inhibitor EC_{50} values were virtually identical with those obtained with HSP90 (**Supplementary Fig. 2**). Thus, this co-chaperone is equally effective as a thermodynamic sensor of small molecule–kinase interactions.

Finally, we asked whether the assay could be broadened to other types of target proteins, other types of compounds, and to chaperones that act in a distinct manner from HSP90. We focused on two steroid hormone receptors that are known to associate with chaperones: the androgen receptor (AR) and the glucocorticoid receptor (GR)[22]. Although we detected an interaction between HSP90 and these receptors in our assay, the interaction was not strong enough to give a reliable change in signal upon ligand binding. We asked, therefore, if the interaction between these receptors and the HSP70 chaperone might be used as the sensor. We created a 293T cell line that stably expresses a *Renilla*-HSC70 (*HSPA8*) fusion protein and transfected them with 3xFLAG-tagged AR or GR expression vectors. When their respective ligands were added to culture medium before cell lysis, HSC70 dissociated from AR and from GR. Again, the potency of both ligands as measured by the chaperone assay was comparable to known potencies[23,24] and highly specific for the correct ligand-receptor pairing (**Fig. 4c**,**d**). HSP70 acts at an earlier stage than HSP90 in the maturation cycle of these clients[22]. Thus, these results establish that distinct steps in protein folding pathways can be exploited as thermodynamic sensors, broadening the potential application of our assay.

Kinome-wide profiling: ATP-competitive inhibitors

Having established the applicability of the assay for single kinases, we asked if the assay could be used more systemically to profile inhibitor specificities and discover new drug targets. In our efforts to understand HSP90 client protein specificity, we had previously assembled a panel of 420 full-length kinase clones (representing 355 unique wild-type kinases and various splice isoforms)[1]. We expanded this collection with another 135 mutant kinase clones of interest in drug discovery efforts. This addition consisted of 29 translocations (involving 14 different kinase domains), 31 oncogenic mutants (in 9 different kinases), 43 drug-resistant kinase variants (of three kinases), all of which are associated with oncogenic phenotypes. We also included 32 variants in 13 different kinases that have been causally linked to dominant Mendelian diseases (**Supplementary Table 1**). About 70% of these new constructs interacted with HSP90 and CDC37 and could thus be tested in our assay, compared to 60% of the original kinase panel.

First, we transfected our kinase collection into *Renilla*-HSP90 and CDC37-*Renilla* cells (each in duplicate) and quantitatively measured each kinase-HSP90 and kinase-CDC37 interaction by LUMIER with BACON. Consistent with our previous results[1], the assay was highly reproducible with an R^2 value of 0.98 between replicates (**Fig. 5a** and **Supplementary Fig. 3**). Next, we repeated the assay in quadruplicate, but treated the cells with 5 μM staurosporine (two replicates) or DMSO (two replicates) for 1 h before cell lysis. Staurosporine is a promiscuous kinase inhibitor targeting all kinase families[4], and thus would be expected to affect a large fraction of HSP90-kinase interactions. Indeed, staurosporine treatment led to a significant reduction in 45% of HSP90-kinase interactions (**Fig. 5b**).

Having established the robustness and reproducibility of the assay platform, we screened 30 small molecules at 5 μM against our entire kinase collection. These included kinase inhibitors approved by the US Food and Drug Administration, inhibitors currently in clinical trials, and compounds in preclinical development (**Supplementary Table 1**). The compounds represented all types of kinase inhibitors: active (type I) and inactive (type II) conformation binders, allosteric (type III) modulators and irreversible inhibitors. HSP90 and CDC37 interaction profiles with kinases correlate very strongly[1] and the EC_{50} values derived with both interaction assays are nearly identical (see above), but the signal-to-noise ratio was slightly better with the CDC37-*Renilla* cell line (data not shown). Therefore, most inhibitors were profiled with CDC37 as the sensor (**Supplementary Table 1**).

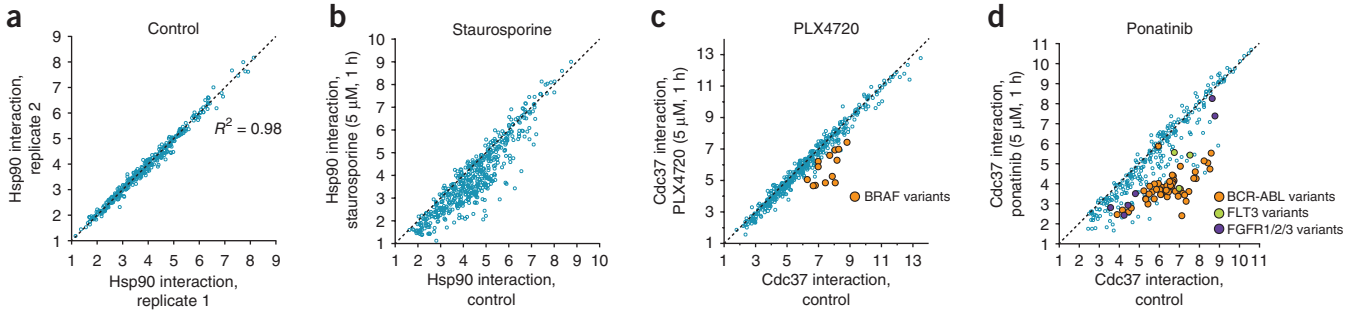

Figure 5 Profiling kinase inhibitor specificities with the chaperone interaction assay. (**a**) 3xFLAG-tagged kinase collection (blue circles) was used to transfect in duplicate 293T cells stably expressing the *Renilla*-Hsp90 fusion protein. Two days later, kinase-Hsp90 interactions were measured with LUMIER with BACON assay. Kinase-Hsp90 interaction strength is calculated as $\log_2$[Hsp90/kinase]. (**b**) The nonspecific kinase inhibitor staurosporine affects a large fraction of kinase-Hsp90 interactions. Kinases were transfected in quadruplicate into *Renilla*-Hsp90 cells. Two of the replicates were treated with 5 μM staurosporine and two with DMSO for 1 h before lysis and LUMIER with BACON assay. (**c**) PLX4720 is a specific BRAF inhibitor. 293T cells stably expressing CDC37-*Renilla* luciferase fusion protein and transfected with 3xFLAG tagged kinases were treated with PLX4720 (5 μM, 1 h) or vehicle before the assay. PLX4720 specifically affects the interactions between BRAF variants (orange circles) and CDC37. (**d**) Ponatinib targets multiple kinases. The experiment was performed as in **c**, except that cells were treated with 5 μM ponatinib for 1 h before cell lysis and LUMIER with BACON assay. The known targets of ponatinib, ABL1, FLT3 and FGFR family receptors are indicated as orange, green and purple circles, respectively.

In all but four cases, we identified the primary target of the inhibitor if it was among the HSP90- or CDC37-interacting kinases in our collection (**Supplementary Table 1** and **Supplementary Discussion**). For example, chaperone profiling identified wild-type and mutant BRAF as specific targets of PLX4720 (**Fig. 5c**). Similarly, ponatinib has been reported as a potent BCR-ABL[15], pan-FGFR[25] and FLT3 inhibitor[26]. Consistent with this, we identified all three as prominent ponatinib targets (**Fig. 5d**). For PLX4720, we identified 17 additional kinases as potential targets, and for ponatinib, 48. It is possible that some of these represent indirect activities (e.g., upstream kinase activation) that could affect chaperone binding, but this is unlikely to be a general confounding factor. For example, receptor tyrosine kinase inhibitors did not affect the chaperone interactions of downstream kinases (e.g., MEK and ERK family kinases), even though their activity states must have been affected.

For all inhibitors, we measured inhibitor EC_{50} values for up to ten of the most prominent kinase hits (see **Supplementary Fig. 4** for examples and **Supplementary Table 2** for all data). Previously established *in vitro* specificity profiles (KINOMEscan) were available for nine of the inhibitors[5,7]. For five of these (crizotinib, GDC0879, HG-6-64-1, PLX4720, and sorafenib (Nexavar)), there was a statistically significant overlap between our data and previously published data sets ($P < 0.0001$, $P < 0.0001$, $P = 0.0014$, $P = 0.0011$ and $P < 0.001$, respectively; **Supplementary Fig. 5**). For two inhibitors (EPHB2 inhibitor ALW-II-49-7 and BTK inhibitor QL-X-138) the overlap was not statistically significant, as only a few of the previously identified *in vitro* targets were profiled with our assay (**Supplementary Fig. 5**).

For staurosporine, a larger number of targets had been identified in previous *in vitro* investigations. To address this discrepancy, we chose six such kinases for further study. We transfected 293T cells with the kinases, treated cells with staurosporine, and asked whether staurosporine altered kinase autophosphorylation, a surrogate for kinase activity. For four of the six, autophosphorylation changes were consistent with our results from the primary screen (**Supplementary Fig. 6a**). Thus, for these kinases, our *in vivo* LUMIER assay reflected inhibitor specificity better than former *in vitro* assays. Autophosphorylation of one kinase was affected by the inhibitor, but when we retested it by LUMIER, it proved to be a *bone fide* target by this assay, too. Thus, it was simply a false negative in the primary screen. Only one kinase, FLT4, showed a discordant pattern. It was not displaced from CDC37, even though its phosphotyrosine content decreased with staurosporine. Because we have found FLT4 to be a target of several other kinase inhibitors using our assay, this kinase is not intrinsically incompatible with the LUMIER assay. Instead, staurosporine might have an unusual mode of binding to FLT4 or the kinase might be transphosphorylated by a separate, staurosporine-sensitive kinase. Finally, we tested one kinase that was not previously identified as a staurosporine target but did score in our screen—JAK1. The effects of staurosporine on JAK1 autophosphorylation confirmed that it is indeed a target of this compound (**Supplementary Fig. 6b**). Thus, the chaperone interaction assay is a robust method for identifying biologically relevant kinase inhibitor targets in a high-throughput manner.

To more critically evaluate the relevance of our results to cellular physiology, we compared the measured EC_{50} values to previously published cellular potencies. We included only assays in which the cellular potency could be unequivocally attributed to a specific drug-target interaction (e.g., excluding sensitivity data for cancer cell lines that likely contain multiple genetic lesions). Such data were available for 40 drug-target pairs targeted by ten diverse compounds (**Supplementary Table 3**). The cellular potency of these compounds spanned almost five orders of magnitude (100 pM to 5 μM). Their measured EC_{50} values from the chaperone interaction assay strongly correlated with their cellular potencies (logarithmic R^2 0.74, $P < 0.0001$, linear R^2 0.59, $P < 0.0001$; **Supplementary Fig. 7**). The robust correlation between the two very different assays further demonstrates the ability of the LUMIER assay to address cellular physiology.

Kinome-wide profiling: allosteric modulators

As noted above, allosteric kinase inhibitors are thought to be more specific than ATP-competitive inhibitors, as they target nonconserved pockets[27]. Although this concept is intuitively reasonable, it has been challenging to systematically test it *in vivo*. To address this deficiency, we used our chaperone sensor assay to profile six allosteric inhibitors and one allosteric activator. All proved to be exquisitely specific. For example, allosteric AKT inhibitors MK-2206 and Kin001-102, which bind the interface between the AKT kinase domain and its pleckstrin-homology (PH) domain[27], only targeted the AKT family kinases (**Supplementary Fig. 8**). The allosteric MEK inhibitor trametinib (MEKINIST) did not affect any wild-type kinases that interacted with CDC37. (Wild-type MEK1 (MAP2K1) or MEK2 (MAP2K2) do not associate with CDC37 and were not assayed.) However, introducing

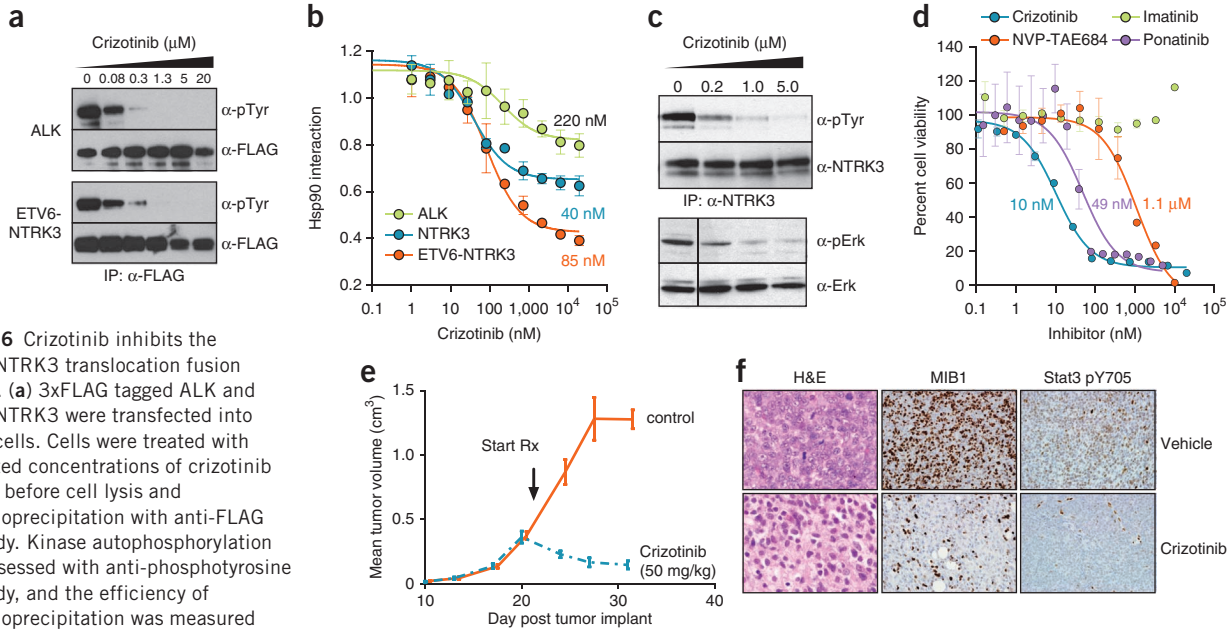

Figure 6 Crizotinib inhibits the ETV6-NTRK3 translocation fusion kinase. (**a**) 3xFLAG tagged ALK and ETV6-NTRK3 were transfected into 293T cells. Cells were treated with indicated concentrations of crizotinib for 1 h before cell lysis and immunoprecipitation with anti-FLAG antibody. Kinase autophosphorylation was assessed with anti-phosphotyrosine antibody, and the efficiency of immunoprecipitation was measured with an anti-FLAG antibody. (**b**) Crizotinib potently disrupts the ETV6-NTRK3–HSP90 interaction. Indicated 3xFLAG tagged kinases were transfected into *Renilla*-Hsp90 cells and the cells were treated with increasing concentrations of crizotinib for 1 h before cell lysis and the LUMIER assay. Relative Hsp90 interaction values (no inhibitor = 1) were fitted to a three-parameter dissociation curve with Graphpad Prism. Error bars, mean ± s.d. (**c**) Crizotinib treatment led to decreased ETV6-NTRK3 phosphorylation and downregulation of downstream MAPK-ERK signaling. MO91 cells were treated with indicated concentrations of crizotinib for 1 h. After cell lysis, ETV6-NTRK3 was immunoprecipitated from the lysate with an anti-NTRK3 antibody and kinase autophosphorylation status was assessed with a phosphotyrosine-specific antibody. The activity MAPK-ERK signaling, downstream of NTRK3, was tested with a phospho-Erk antibody. (**d**) MO91 cells are exceedingly sensitive to crizotinib. MO91 cells were treated with increasing concentrations of the ALK inhibitors crizotinib and NVP-TAE684 or with the ABL1 inhibitors imatinib and ponatinib or 48 h. Cell viability was measured with alamarBlue assay. Error bars, mean ± s.d. (**e**) Regression of MO91-TA xenografts upon crizotinib treatment. Sixteen nude mice were subcutaneously injected with 5×10^6 MO91-TA cells each. When the tumor size reached ~350 mm^3, eight mice were treated with 50 mg/kg crizotinib and eight with vehicle only, using a gavage needle. Tumor size was measured with a caliper. (**f**) Immunohistochemical analysis of crizotinib-treated tumor xenografts. Crizotinib-treated tumors and control tumors were surgically removed from mice and stained with hematoxylin and eosin (left panel) or immunohistochemically stained for proliferation marker MIB1 (middle panel) or for Stat3 phosphorylation at tyrosine 705 (right panel).

destabilizing mutations in MAPK2K2 led to robust CDC37 interaction, which was disrupted by trametinib (**Supplementary Fig. 8**).

Finally, we assayed two that target the ABL1 myr-pocket, GNF-2 and DPH. Again, ABL1 and BCR-ABL were the only kinases whose chaperone interactions were consistently affected by GNF-2 and DPH (**Supplementary Fig. 9a** and **Supplementary Table 2**). We also tested 39 BCR-ABL variants that had been recovered in a screen for imatinib resistance[28]. All but one of these were affected by GNF-2 treatment, but the extent of dissociation from HSP90 varied considerably (**Supplementary Fig. 9b**). Notably, nine of these variants had also been recovered in an independent screen for mutations that confer partial or full resistance to GNF-2 *in vivo*[18]. The GNF-2 resistant clones we profiled were less strongly displaced from HSP90 by GNF-2 than the remaining clones ($P < 0.0001$, Wilcoxon rank sum test; **Supplementary Fig. 9b**). The single variant whose interaction with HSP90 was not affected by GNF-2 (P439T/I502M) contained a mutation in the myr-pocket and had not previously been tested for GNF-2 resistance. To test the resistance of this variant in a biologically meaningful setting, we used BaF/3 cells that had been oncogenically transformed with this variant and were dependent on it for growth and survival. Indeed, as predicted by our assay, these cells were more resistant to GNF-2 than cells transformed with the native BCR-ABL (**Supplementary Fig. 9c**).

These results provide *in vivo* validation for the notion that allosteric modulators are more specific than ATP-competitive kinase inhibitors. Furthermore, the data show that drug-resistant variants can be predicted with high-throughput chaperone profiling.

Crizotinib is a potent inhibitor of ETV6-NTRK3

To demonstrate the translational value of our assay to uncover clinically relevant secondary targets, we focused on crizotinib (Xalkori), a recently approved high-potency inhibitor of the ALK and MET tyrosine kinases[29]. We identified several other tyrosine kinases as potential secondary targets (**Supplementary Table 2**). Some of these had been identified as secondary targets previously by other methods but *in vivo* data existed for only a few[5,7,30]. To test the effect of crizotinib on the tyrosine kinase activity of the potential targets we identified, we assessed the autophosphorylation state of each kinase after a 1-h crizotinib treatment. As expected, crizotinib potently inhibited ALK autophosphorylation (**Fig. 6a**) as well as that of previously reported targets ABL1 and AXL (**Supplementary Fig. 10**). In addition, autophosphorylation of the translocation fusion kinase ETV6-NTRK3 was also markedly reduced by crizotinib (**Fig. 6a**). Although wild-type NTRK3 was among the 146 previously reported *in vitro* targets of the drug[5], ETV6-NTRK3 fusion has previously not been described as an *in vivo* target of crizotinib. Other targets (FES, TESK1, INSRR, EPHA2) were also affected by crizotinib, albeit only at higher concentrations (**Supplementary Fig. 10**). We also measured the EC_{50} of crizotinib for each target with the chaperone interaction assay. The potency of crizotinib in reducing kinase autophosphorylation and its potency in dissociating the kinases from HSP90 were in good agreement (**Fig. 6b** and **Supplementary Fig. 10**).

Notably, crizotinib inhibited the ETV6-NTRK3 translocation fusion kinase in our assay even more potently (EC_{50}: 85 nM) than

it inhibited its primary target ALK (EC_{50}: 220 nM) (**Fig. 6b**). This translocation has been found in pediatric tumors such as fibrosarcomas, mesoblastic nephromas and secretory breast carcinomas[31]. Infantile fibrosarcoma is the most common soft-tissue sarcoma in infants. Despite a generally favorable prognosis, treatment of more advanced tumors can require radical surgery and even amputation[32]. In adults, this translocation has been associated with acute myeloid leukemia[33,34] and a distinct subclass of salivary gland tumors, which occasionally metastasize and have poor outcome[33–35]. Thus, a drug targeting ETV6-NTRK3 might offer a valuable treatment option for these rare but often devastating cancers.

To test the effect of crizotinib on human tumor cells, we chose the M091 cell line, which carries the ETV6-NTRK3 translocation and was derived from a patient with acute myeloid leukemia[36]. Confirming our results from 293T cells, crizotinib potently inhibited endogenous ETV6-NTRK3 autophosphorylation in M091 cells after 1-h treatment (**Fig. 6c**). To determine if crizotinib inhibited signaling downstream of activated NTRK3, we measured the effect of crizotinib on ERK phosphorylation[37]. ERK phosphorylation was reduced in a concentration-dependent manner upon drug treatment (**Fig. 6c**).

Next, we assayed the sensitivity of M091 cell growth and survival to crizotinib. The cells were very sensitive to the drug, with a GI50 in the low nanomolar range (**Fig. 6d**). To exclude the possibility that this was due to inhibition of other known crizotinib targets that could play an important role in M091 biology, we tested three additional inhibitors. NVP-TAE684 inhibits ALK with low nanomolar potency[38]. Yet, it inhibited M091 cell growth only at micromolar concentrations (**Fig. 6d**), suggesting that ALK inhibition is not responsible for crizotinib's growth-inhibitory effect. Similarly, the ABL1 inhibitor imatinib had no effect on M091 proliferation even at high concentrations (**Fig. 6d**). However, another ABL1 inhibitor ponatinib, which we found to also target NTRK3 in our screen (**Supplementary Table 2**), did inhibit the growth of the cells with nanomolar potency. Thus, the effect of crizotinib on M091 cell proliferation is not due to ALK or ABL1 inhibition but is very likely a result of direct inhibition of ETV6-NTRK3.

To evaluate the activity of crizotinib *in vivo* against an ETV6-NTRK3-dependent tumor, we developed a xenograft model in non-obese diabetic-severe combined immunodeficiency (NOD-SCID) mice. Parental M091 cells were passaged as subcutaneous implants through these mice to generate a more highly tumorigenic variant that was adapted to engraft and progress in sufficiently uniform fashion to support testing of drug activity *in vivo*. When explanted in cell culture, these *in vivo*–passaged cells (M091-TA) remained highly sensitive to crizotinib (**Supplementary Fig. 11**) and were used for subsequent experiments evaluating anticancer activity. Three weeks after subcutaneous injection of M091-TA cells, we randomly assigned mice bearing established xenografts to treatment with crizotinib or vehicle control. Crizotinib was administered by oral gavage using a well-tolerated dose of 50 mg/kg once a day. The control treatment group received an equal volume of water on the same schedule. Control-treated tumors rapidly grew to the point where the mice had to be euthanized. In contrast, crizotinib induced tumor regression after only a few days' treatment (**Fig. 6e**).

At the end of the treatment interval, we resected tumor xenografts to examine relevant pharmacodynamic endpoints. Control-treated samples showed dense sheets of tumor cells with overt features of high-grade malignancy: large irregular nuclei with prominent nucleoli, regions of nuclear clearing representing open chromatin, and frequent, easily identified mitotic figures (**Fig. 6f**). By contrast, in crizotinib-treated animals tumor cells were sparse and were embedded in a fibrotic extracellular matrix. Mitoses were very infrequent, nucleoli were inconspicuous and nuclei were small with condensed chromatin, all features of nonproliferating cells (**Fig. 6f**). Immunohistochemistry for two proliferation markers, Ki67 (MIB1) and phospho-histone H3S10, confirmed that crizotinib treatment had markedly reduced proliferation (**Fig. 6f** and **Supplementary Fig. 12**). Moreover, crizotinib treatment caused a sharp decrease in total phosphotyrosine levels in the tumors (**Supplementary Fig. 12**) and specifically in the activated form of STAT3 that is phosphorylated in cells carrying the ETV6-NTRK3 translocation (**Fig. 6f**)[39].

DISCUSSION

Here, we establish that chaperones can be used as 'thermodynamic sensors' for drug–target interactions. We used HSP90, CDC37 and HSC70 as examples of chaperones, and kinases and steroid hormone receptors as examples of drug targets. But it is likely that our approach will prove broadly applicable with other chaperones and other drug targets. The binding of small molecules to their targets generally leads to thermodynamic stabilization of those targets[40]. If the target proteins are in equilibrium between their fully folded and partially folded chaperone-bound conformations, drug binding will lead to decreased chaperone association. Chaperones associate with a large fraction of proteins in all organisms even at their steady states[1,41,42], and, as we have shown, proteins that do not associate with them in this manner can be readily engineered to do so.

Our assay depends neither on the enzymatic activity of the target protein nor on a particular binding pocket in the target. Thus, it should be well suited for the pursuit of drugs for targets that have been notoriously difficult to assay in biologically relevant contexts, including E3 ligases[1], transcription factors[1], and diverse protein-protein interactions. Our method is amenable to high-throughput automation, bridging the gap between the more traditional high-throughput *in vitro* methods and lower throughput *in vivo* approaches in drug discovery.

We illustrated the utility of chaperone profiling by surveying kinase inhibitor specificities *in vivo*. Compared to other available methods for kinase inhibitor profiling[5–7], our approach has several advantages. First, it uses full-length kinases in their native cellular environment, in the context of physiological post-translational modifications, conformational switches and cellular interactors. Although the expression levels of the kinases in our assay are higher than endogenous levels, the strong correlation between our results and *in vivo* potency suggests that this is not a generally confounding factor. With the use of lentiviral delivery systems, it should be readily adaptable to any cell type in cases where a particular cellular context is required (e.g., stem cells, neuronal cells). Second, kinases are assayed at physiological ATP concentrations. As most kinase inhibitors are ATP-competitive, the difference between *in vitro* and *in vivo* ATP concentrations often leads to substantial changes in cellular potency. Third, the assay is compatible with allosteric inhibitors and activators, in contrast to other *in vivo* approaches[11,12]. For example, neither GNF-2 nor MK2206 would have been identified in an *in vitro* screen using ABL1 or AKT1 kinase domains only, as the inhibitors absolutely require the kinases' regulatory domains for function[27].

Finally, we established that the assay can be used to discover clinically relevant drug targets. NTRK3 and its translocation fusion variant ETV6-NTRK3 proved to be prominent targets of crizotinib. Crizotinib inhibited ETV6-NTRK3 with nanomolar potency and treatment of ETV6-NTRK3-dependent xenografts with crizotinib led to dramatic regression of tumors. These results suggest that it might be worth testing crizotinib as a therapeutic agent against cancers driven by the ETV6-NTRK3 translocation. Crizotinib is already approved for

use in the treatment of certain lung cancers. Recommended dosing parameters with a good safety profile for children have already been established[43]. Thus it should be possible to translate these findings rapidly to efficacy trials in selected pediatric malignancies such as infantile fibrosarcoma. Furthermore, given the intense interest in repurposing drugs and expanding the scope of druggable targets, the ease and reproducibility of our assay should have broad application in drug development.

METHODS

Methods and any associated references are available in the online version of the paper.

Note: Supplementary information is available in the online version of the paper.

ACKNOWLEDGMENTS

We thank the Lindquist laboratory members for valuable discussions and comments on the manuscript. We also thank M. Azam (Cincinnati Children's Hospital Medical Center) for providing mutant BCR-ABL clones and P. Thiru, I. Barrasa and G. Bell (Whitehead Institute) for help with primer design and statistical analysis. M.T. was supported by Human Frontier Science Programme long-term fellowship. S.L. is a Howard Hughes Medical Institute investigator. Support for this study was also provided by the US National Institutes of Health (NIH) Genomics Based Drug Discovery-Driving Medical Projects grant UL1-DE019585, administratively linked to NIH grants RL1-GM084437, RL1-CA133834 and RL1-HG004671.

AUTHOR CONTRIBUTIONS

M.T. and S.L. planned the project. M.T. designed the experiments, developed the assay, performed the experiments together with I.K., and analyzed the data. Xenograft experiments were done by L.W., and S.S. performed immunohistochemistry on tumor samples. J.Z. tested BCR-ABL variants for GNF-2 sensitivity in BaF/3 cells. J.Z., Q.L. and N.S.G. synthesized and provided kinase inhibitors and helped design experiments. M.T. and S.L. wrote the paper with input from all co-authors.

COMPETING FINANCIAL INTERESTS

The authors declare competing financial interests: details are available in the online version of the paper.

1. Taipale, M. *et al.* Quantitative analysis of HSP90-client interactions reveals principles of substrate recognition. *Cell* **150**, 987–1001 (2012).
2. Goldstein, D.M., Gray, N.S. & Zarrinkar, P.P. High-throughput kinase profiling as a platform for drug discovery. *Nat. Rev. Drug Discov.* **7**, 391–397 (2008).
3. Karaman, M.W. *et al.* A quantitative analysis of kinase inhibitor selectivity. *Nat. Biotechnol.* **26**, 127–132 (2008).
4. Fabian, M.A. *et al.* A small molecule-kinase interaction map for clinical kinase inhibitors. *Nat. Biotechnol.* **23**, 329–336 (2005).
5. Davis, M.I. *et al.* Comprehensive analysis of kinase inhibitor selectivity. *Nat. Biotechnol.* **29**, 1046–1051 (2011).
6. Fedorov, O. *et al.* A systematic interaction map of validated kinase inhibitors with Ser/Thr kinases. *Proc. Natl. Acad. Sci. USA* **104**, 20523–20528 (2007).
7. Anastassiadis, T., Deacon, S.W., Devarajan, K., Ma, H. & Peterson, J.R. Comprehensive assay of kinase catalytic activity reveals features of kinase inhibitor selectivity. *Nat. Biotechnol.* **29**, 1039–1045 (2011).
8. Bain, J. *et al.* The selectivity of protein kinase inhibitors: a further update. *Biochem. J.* **408**, 297–315 (2007).
9. Eck, M.J. & Manley, P.W. The interplay of structural information and functional studies in kinase drug design: insights from BCR-Abl. *Curr. Opin. Cell Biol.* **21**, 288–295 (2009).
10. Posy, S.L. *et al.* Trends in kinase selectivity: insights for target class-focused library screening. *J. Med. Chem.* **54**, 54–66 (2011).
11. Bantscheff, M. *et al.* Quantitative chemical proteomics reveals mechanisms of action of clinical ABL kinase inhibitors. *Nat. Biotechnol.* **25**, 1035–1044 (2007).
12. Patricelli, M.P. *et al.* In situ kinase profiling reveals functionally relevant properties of native kinases. *Chem. Biol.* **18**, 699–710 (2011).
13. Barrios-Rodiles, M. *et al.* High-throughput mapping of a dynamic signaling network in mammalian cells. *Science* **307**, 1621–1625 (2005).
14. Shah, N.P. *et al.* Overriding imatinib resistance with a novel ABL kinase inhibitor. *Science* **305**, 399–401 (2004).
15. O'Hare, T. *et al.* AP24534, a pan-BCR-ABL inhibitor for chronic myeloid leukemia, potently inhibits the T315I mutant and overcomes mutation-based resistance. *Cancer Cell* **16**, 401–412 (2009).
16. Waldron, T.T. & Murphy, K.P. Stabilization of proteins by ligand binding: application to drug screening and determination of unfolding energetics. *Biochemistry* **42**, 5058–5064 (2003).
17. Vaughan, C.K. *et al.* Structure of an Hsp90-Cdc37-Cdk4 complex. *Mol. Cell* **23**, 697–707 (2006).
18. Zhang, J. *et al.* Targeting Bcr-Abl by combining allosteric with ATP-binding-site inhibitors. *Nature* **463**, 501–506 (2010).
19. Yang, J. *et al.* Discovery and characterization of a cell-permeable, small-molecule c-Abl kinase activator that binds to the myristoyl binding site. *Chem. Biol.* **18**, 177–186 (2011).
20. Iacob, R.E., Zhang, J., Gray, N.S. & Engen, J.R. Allosteric interactions between the myristate- and ATP-site of the Abl kinase. *PLoS ONE* **6**, e15929 (2011).
21. Xu, W. *et al.* Surface charge and hydrophobicity determine ErbB2 binding to the Hsp90 chaperone complex. *Nat. Struct. Mol. Biol.* **12**, 120–126 (2005).
22. Picard, D. Chaperoning steroid hormone action. *Trends Endocrinol. Metab.* **17**, 229–235 (2006).
23. Couture, P., Theriault, C., Simard, J. & Labrie, F. Androgen receptor-mediated stimulation of 17 beta-hydroxysteroid dehydrogenase activity by dihydrotestosterone and medroxyprogesterone acetate in ZR-75–1 human breast cancer cells. *Endocrinology* **132**, 179–185 (1993).
24. Adcock, I.M., Nasuhara, Y., Stevens, D.A. & Barnes, P.J. Ligand-induced differentiation of glucocorticoid receptor (GR) trans-repression and transactivation: preferential targetting of NF-kappaB and lack of I-kappaB involvement. *Br. J. Pharmacol.* **127**, 1003–1011 (1999).
25. Gozgit, J.M. *et al.* Ponatinib (AP24534), a multitargeted pan-FGFR inhibitor with activity in multiple FGFR-amplified or mutated cancer models. *Mol. Cancer Ther.* **11**, 690–699 (2012).
26. Gozgit, J.M. *et al.* Potent activity of ponatinib (AP24534) in models of FLT3-driven acute myeloid leukemia and other hematologic malignancies. *Mol. Cancer Ther.* **10**, 1028–1035 (2011).
27. Dar, A.C. & Shokat, K.M. The evolution of protein kinase inhibitors from antagonists to agonists of cellular signaling. *Annu. Rev. Biochem.* **80**, 769–795 (2011).
28. Azam, M., Latek, R.R. & Daley, G.Q. Mechanisms of autoinhibition and STI-571/imatinib resistance revealed by mutagenesis of BCR-ABL. *Cell* **112**, 831–843 (2003).
29. Kwak, E.L. *et al.* Anaplastic lymphoma kinase inhibition in non-small-cell lung cancer. *N. Engl. J. Med.* **363**, 1693–1703 (2010).
30. Zou, H.Y. *et al.* An orally available small-molecule inhibitor of c-Met, PF-2341066, exhibits cytoreductive antitumor efficacy through antiproliferative and antiangiogenic mechanisms. *Cancer Res.* **67**, 4408–4417 (2007).
31. Lannon, C.L. & Sorensen, P.H. ETV6-NTRK3: a chimeric protein tyrosine kinase with transformation activity in multiple cell lineages. *Semin. Cancer Biol.* **15**, 215–223 (2005).
32. Orbach, D. *et al.* Infantile fibrosarcoma: management based on the European experience. *J. Clin. Oncol.* **28**, 318–323 (2010).
33. Eguchi, M. *et al.* Fusion of ETV6 to neurotrophin-3 receptor TRKC in acute myeloid leukemia with t(12;15)(p13;q25). *Blood* **93**, 1355–1363 (1999).
34. Kralik, J.M. *et al.* Characterization of a newly identified ETV6-NTRK3 fusion transcript in acute myeloid leukemia. *Diagn. Pathol.* **6**, 19 (2011).
35. Skalova, A. *et al.* Mammary analogue secretory carcinoma of salivary glands, containing the ETV6-NTRK3 fusion gene: a hitherto undescribed salivary gland tumor entity. *Am. J. Surg. Pathol.* **34**, 599–608 (2010).
36. Okabe, M. *et al.* Megakaryocytic differentiation of a leukemic cell line, MC3, by phorbol ester: induction of glycoprotein IIb/IIIa and effects on expression of IL-6, IL-6 receptor, mpl and GATA genes. *Leuk. Res.* **19**, 933–943 (1995).
37. Tognon, C. *et al.* The chimeric protein tyrosine kinase ETV6-NTRK3 requires both Ras-Erk1/2 and PI3-kinase-Akt signaling for fibroblast transformation. *Cancer Res.* **61**, 8909–8916 (2001).
38. Galkin, A.V. *et al.* Identification of NVP-TAE684, a potent, selective, and efficacious inhibitor of NPM-ALK. *Proc. Natl. Acad. Sci. USA* **104**, 270–275 (2007).
39. Gadd, S. *et al.* Mediators of receptor tyrosine kinase activation in infantile fibrosarcoma: a Children's Oncology Group study. *J. Pathol.* **228**, 119–130 (2012).
40. Chaires, J.B. Calorimetry and thermodynamics in drug design. *Annu. Rev. Biophys.* **37**, 135–151 (2008).
41. Gong, Y. *et al.* An atlas of chaperone-protein interactions in *Saccharomyces cerevisiae*: implications to protein folding pathways in the cell. *Mol. Syst. Biol.* **5**, 275 (2009).
42. Kerner, M.J. *et al.* Proteome-wide analysis of chaperonin-dependent protein folding in *Escherichia coli*. *Cell* **122**, 209–220 (2005).
43. Mosse, Y.P. *et al.* Efficacy of crizotinib in children with relapsed/refractory ALK-driven tumors including anaplastic large cell lymphoma and neuroblastoma: a Children's Oncology Group phase I consortium study. *J. Clin. Oncol.* **Supplement** Abstract 9500 (2012).

ONLINE METHODS

Kinase clones. The majority of the kinase collection has been described previously[1]. Additional kinases were amplified from cDNA and cloned into pDONR221 entry vector, and subsequently transferred into a pcDNA3.1-based expression vector with a cytomegalovirus promoter and a C-terminal 3xFLAG-V5 tag, using Gateway LR clonase. Kinase mutants were created with site-directed mutagenesis, except for BCR-ABL alleles, which were amplified from retroviral vectors (kindly provided by M. Azam) and cloned into the expression vector with Gateway cloning. All mutations were verified by Sanger sequencing. Coordinates for the translocation breakpoints were downloaded from TICdb[44] and the translocations were created with fusion PCR[45]. Translocation breakpoints were verified by Sanger sequencing.

LUMIER with BACON and inhibitor profiling. LUMIER with BACON was done as previously described[1]. To assay compound EC_{50} values, 3xFLAG tagged kinases (or steroid hormone receptors) were used to transfect stable 293T reporter cell lines (*Renilla*-HSP90AB1, CDC37-*Renilla* or *Renilla*-HSPA8) in 6-well or 12-well plate format. Next day, the cells were split into 96-well plates, and 24 h later the cells were treated with a threefold dilution series of the inhibitor in triplicate for 1 h before cell lysis and the LUMIER assay.

Renilla-HSP90AB1 and CDC37-*Renilla* cell lines have been described earlier[1]. The stable polyclonal 293T cell line expressing *Renilla*-HSPA8 was created with lentiviral infection. The expression construct contained a codon-optimized *Renilla* luciferase fused to the N terminus of human HSPA8 (Hsc70), separated by a glycine-serine rich linker.

To profile kinase inhibitor specificities, we transfected each kinase into the reporter cell line in quadruplicate using polyethylenimine (branched PEI, Sigma-Aldrich 408727). Two days after transfection, two sets of transfections were treated with 5 μM inhibitor and two with vehicle (DMSO) only for 1 h. LUMIER assay was performed on 384-well plates as previously described[1].

Statistical analysis. The quantitative chaperone-client interaction was calculated as the $\log_2$[luminescence]-$\log_2$[ELISA], and normalized such that weakest interactions had an interaction score of 0-1. Kinases for which the luminescence from Hsp90 or Cdc37 was weaker than twofold over negative control (3xFLAG-tagged EGFP) were classified as non-interactors and excluded from analysis.

Kinase inhibitor profiling data were analyzed with the Bioconductor package in R. Duplicate data sets were median-normalized and differential response in treated versus control samples was assayed by a moderated *t*-test as implemented in the limma package in R. Kinases were classified as inhibitor targets if the change in Hsp90 or Cdc37 interaction upon inhibitor treatment was statistically significant ($P < 0.005$). Compounds that bind the fully folded kinase domain are not expected to increase kinase-chaperone interactions; rather, these events represent variation (noise) in the assay. Therefore, if there were more than three kinases that increased their interaction with Hsp90 or Cdc37 upon drug addition with the $P < 0.005$ cutoff, a more stringent cutoff of $P < 0.001$ was applied.

BaF/3 cell proliferation assay. The interleukin (IL)-3–dependent murine pro-B cell line Ba/F3 was maintained in RPMI-1640 medium supplemented with 10% FBS and 10 U/ml recombinant murine IL-3 (Roche). Mutant BCR-ABL–expressing Ba/F3 cells were generated as previously described[46]. Wild-type BCR-ABL–expressing Ba/F3 cells and mutant BCR-ABL–expressing cell lines were maintained in RPMI-1640 medium with 10% FBS. For cellular proliferation assays, cells (0.4×10^6/ml) were plated in duplicate in 96-well plates containing increasing drug concentrations (0.005–10 μM). After incubation at 37 °C in 5% CO2 for 48 h, the effect of the compounds on cell viability was determined by the CellTiter Glo cell viability assay (Promega).

Xenografts. Tumor volumes (mm^3) were calculated by measuring the length (long dimension in centimeters) and width (short dimension) of each mass with a caliper and then using the following standard formula to estimate volume: (length × width × width) × 0.52 × 1,000. Tumor size was measured by a lab technical research associate who was blinded to the treatment groups.

Experimental groups consisted of eight mice per treatment. Cells were inoculated subcutaneously with a 27g needle in a 50/50 mix of PBS and Matrigel in the right inguinal region of each mouse. Daily treatment was begun about 3 weeks later when the average tumor volume across mice had reached ~350 mm^3. Mice were treated orally with crizotinib using a gavage needle as per standard practice.

Immunohistochemistry. Tissue sections were deparaffinized and rehydrated through xylene and graded alcohols. Endogenous peroxidase activity was quenched by incubating the sections for 15 min with 3% hydrogen peroxide in 100% alcohol (1:1). Antigen retrieval was performed with Dako target retrieval solution, pH 6.0 (citrate) or 8.0 (EDTA) in a pressure cooker (120 °C ± 2 °C) for 30 s at 15 ± 5 p.s.i. Sections were incubated for either 40 min at room temperature (Ki67, phospho-tyrosine) or 4 °C overnight (pSTAT3 Y705, phospho-histone H3S10). Application of the secondary antibodies was followed by incubation for 30 min with Dako Labeled Polymer-HRP goat anti-rabbit IgG for all of above antibodies except phospho-tyrosine for which M.O.M. kit was applied (Vector laboratories, PK-2200). The sections were then visualized with 3, 3′–diaminobenzidine (DAB) plus substrate chromogen, which results in a brown-colored precipitate at the antigen site. Mayer hematoxylin was used for counterstaining.

Reagents. Kinase inhibitors were purchased from Chemietek (Indianapolis, IN), Selleck (Houston, TX), Sigma-Aldrich (St. Louis, MO), or synthesized in the Gray laboratory. All inhibitors were dissolved in DMSO. Antibodies were purchased from Sigma (anti-FLAG M2 F1804, 1:3,000 WB, 1:100 ELISA, anti-FLAG M2 affinity resin F2426), Santa Cruz (anti-TrkC N-13 sc-47520, 1:1,000, western blot), Cell Signaling (anti-pTyr 9411, 1:3,000, western blot; anti-pErk 4370, anti-Erk 4695, both 1:1,000, western blot), and Abcam (anti-DDDDK ab1278, 1:10,000 ELISA).

44. Novo, F.J., de Mendibil, I.O. & Vizmanos, J.L. TICdb: a collection of gene-mapped translocation breakpoints in cancer. *BMC Genomics* **8**, 33 (2007).
45. Atanassov, I.I., Etchells, J.P. & Turner, S.R. A simple, flexible and efficient PCR-fusion/Gateway cloning procedure for gene fusion, site-directed mutagenesis, short sequence insertion and domain deletions and swaps. *Plant Methods* **5**, 14 (2009).
46. Koh, E.Y., Chen, T. & Daley, G.Q. Novel retroviral vectors to facilitate expression screens in mammalian cells. *Nucleic Acids Res.* **30**, e142 (2002).

doi:10.1038/nbt.2620